INTERNATIONAL JOURNAL FOR NUMERICAL METHODS IN FLUIDS
Int. J. Numer. Meth. Fluids 2010; **62**:355–373
Published online 16 April 2009 in Wiley InterScience (www.interscience.wiley.com). DOI: 10.1002/fld.2017

Fluid dynamic numerical simulation coupled with heat transfer and reaction in the tubular reactor of industrial cracking furnaces

Chufu Li[1], Tong Qiu[1], Bingzhen Chen[1,*,†], Liang Tian[2], Bangyong Song[2] and Jichun Li[2]

[1]*Department of Chemical Engineering, Tsinghua University, Beijing 100084, China*
[2]*Lanzhou Chemical Research Center, Petrochina, Lanzhou 730060, China*

SUMMARY

The thermal cracking furnace is the heart of the ethylene production process in a petrochemical plant. This paper presents a comprehensive mathematical model containing equations for mass, momentum and heat transfer combined with Kumar molecular kinetic model to describe dynamic behaviors of fluid flow, heat transfer and reaction in the tubular reactor of thermal cracking furnaces. The 'flow-reaction' decomposition strategy is adopted to solve the complex model for implementing the fluid dynamic simulation coupled with heat transfer and reaction in the tubular reactor by a conventional procedure. The proposed mathematical model and the decomposition algorithm are successfully applied to the fluid dynamic simulation in the tubular reactor of a millisecond industrial cracking furnace. The results of dynamic simulation reveal the various transient behaviors of fluid flow, temperature change and species content variation in the tubular reactor under the step disturbance of inlet feedrate. Finally, the performance of the decomposition algorithm is also investigated. Copyright © 2009 John Wiley & Sons, Ltd.

Received 30 August 2008; Revised 15 January 2009; Accepted 16 January 2009

KEY WORDS: cracking furnace; tubular reactor; naphtha pyrolysis; decomposition strategy; compressible flow; finite difference methods

1. INTRODUCTION

The ethylene production process is one of the most important aspects of a petrochemical plant and the thermal cracking furnace is the heart of the process. For finding an optimal operating

*Correspondence to: Bingzhen Chen, Department of Chemical Engineering, Tsinghua University, Beijing 100084, China.
†E-mail: dcecbz@tsinghua.edu.cn

Contract/grant sponsor: National Scientific and Technical Supporting Programs; contract/grant number: 611408001

strategy, it is necessary to perform a static simulation. Several packages have been developed to implement a static simulation of thermal cracking furnaces based on radical reaction mechanisms [1–4]. Generally, pyrolysis reactions are coupled with heat transfer and fluid flow in the thermal cracking furnace. Niaei *et al.* [5] carried out the steady-state combined simulation of heat transfer and pyrolysis reactions in industrial cracking furnaces using a rigorous kinetic model. Heynderickx *et al.* [6] adopted computational fluid dynamics (CFD) to investigate three-dimensional flow patterns in the thermal cracking furnace with long-flame burners for its design. Lan *et al.* [7] developed a comprehensive mathematical model with CFD and performed steady numerical simulation of complex transfer and reaction for the design of ethylene furnaces using Fluent package based on a molecular kinetic model.

However, for understanding dynamic characteristics and evaluating control strategies of thermal cracking furnaces, it is necessary to perform a dynamic simulation. Shahrokhi and Nedjati [8] developed a reduced dynamic model for the propane thermal cracking reactor only considering transient gas temperatures and component contents to evaluate the performance of a control scheme. Masouemi *et al.* [9] used the dynamic model proposed by Shahrokhi and Nedjati [8] to investigate the control strategies of a naphtha thermal cracking furnace in a pilot plant. Ghashghaee and Karimzadeh [10] developed a transient model to describe and predict the unsteady-state heat transfer behavior of cracking furnaces during start-up.

In these researches, the transient fluid flow is neglected in the dynamic mathematical models for the thermal cracking process. Recently, fluid dynamic simulation coupled with chemical reactions in reactors has been concerned by some researchers [11–13]. Based on the previous work [14] focusing on the static simulation of industrial cracking furnaces, this paper presents a comprehensive mathematical model containing equations for mass, momentum and heat transfer combined with a molecular kinetic model to describe unsteady-state behaviors of fluid flow, heat transfer and reaction in the tubular reactor of industrial cracking furnaces. Subsequently, the 'flow-reaction' decomposition strategy is adopted to solve the model for performing the fluid dynamic simulation coupled with heat transfer and reaction in the tubular reactor.

2. PROCESS DESCRIPTION

Industrial production of ethylene is based on thermal cracking of petroleum hydrocarbons with steam, which is commonly called pyrolysis or steam cracking. Hydrocarbon feed mixed with process steam is introduced into the cracking coils with short residence time and at a high temperature. The homogeneous cracking reactions are endothermic and energy input is required in order to reach the gas temperature as high as 800–900°C at the coil outlet. The required energy is supplied by a thermal cracking furnace. In fact, hydrocarbon feed is mixed with steam in the convection section of the furnace and the temperature of the mixture is raised to the cracking temperature. The mixture is then fed into the radiant section (tubular reactor) of the furnace, where the hydrocarbon is cracked to combinations of olefins, aromatics, pyrolysis fuel oil and other heavier hydrocarbons. Upon leaving the radiant section of the furnace, the cracked gas is cooled rapidly to stop the undesired reactions [9].

Naphtha is the most widely used feed materials for the thermal cracking furnace. Naphtha is a mixture of complex hydrocarbon materials, which ranges mostly from C5 to C10 paraffins. In the tubular reactor, numerous cracking reactions occur to produce ethylene and propylene. Generally, naphtha pyrolysis is considered to follow a free radical reaction mechanism [15]. However, the

DOI: 10.1002/fld

free radical reaction model will result in sets of differential equations that are difficult to solve. Hence, the molecular kinetic model proposed by Kumar and Kunzru [16] is adopted in this work. The model contains 18 species and 22 reactions, and it has been validated by some researchers [14, 17, 18].

3. MATHEMATICAL MODEL

For dynamic simulation in the tubular reactor of industrial cracking furnaces, the following assumptions have been considered for the mathematical model:

1. One-dimensional flow and plug flow.
2. Radial concentration gradients and axial dispersion are negligible.
3. Ideal gas behavior.
4. Coke deposition is neglected in a short dynamic response time.

The model equations are subdivided into three blocks: flow, energy and reaction.

3.1. Flow model equations

The one-dimensional flow model in pipes proposed by Malik *et al.* [19] is used here. Continuity equation for the cracking gas in the tubular reactor is

$$\frac{\partial P}{\partial t}+\frac{\mathrm{RT}}{\overline{M}S}\frac{\partial G}{\partial l}=0 \tag{1}$$

where

$$\overline{M}=\frac{\sum_{m\in\mathrm{COM}}N_mM_m+N_{\mathrm{H_2O}}M_{\mathrm{H_2O}}}{\sum_{m\in\mathrm{COM}}N_m+N_{\mathrm{H_2O}}},\quad G=\sum_{m\in\mathrm{COM}}N_mM_m+N_{\mathrm{H_2O}}M_{\mathrm{H_2O}}$$

Momentum equation for the cracking gas in the tubular reactor is

$$\frac{\partial G}{\partial t}+S\frac{\partial P}{\partial l}+\frac{\mathrm{RT}}{\overline{M}S}\frac{\partial(G^2/P)}{\partial l}+\frac{1}{2}\frac{\mathrm{RT}feG|G|}{\overline{M}DSP}=0 \tag{2}$$

where $f=0.01227+(0.0543/Re^{0.38})$ [20], $Re=GD/S\overline{v}$, $\overline{v}=\sum_{m\in\mathrm{COM}}(v_mN_mM_m^{0.5})/\sum_{m\in\mathrm{COM}}(N_mM_m^{0.5})$.

The term $(\mathrm{RT}/\overline{M}S)\partial(G^2/P)/\partial l$ complicates the equation while its contribution is almost negligible. Magnitude wise, the term in the above equation is of the order given by

$$\frac{\partial G}{\partial t}:S\frac{\partial P}{\partial l}:\frac{\mathrm{RT}}{\overline{M}S}\frac{\partial(G^2/P)}{\partial l}:\frac{1}{2}\frac{\mathrm{RT}feG|G|}{\overline{M}DSP}=0.1:1.0:0.01:1.0$$

Neglecting the third term, we have Equation (2) as

$$\frac{\partial G}{\partial t}+S\frac{\partial P}{\partial l}+\frac{1}{2}\frac{\mathrm{RT}feG|G|}{\overline{M}DSP}=0 \tag{3}$$

DOI: 10.1002/fld

3.2. Reaction model equations

The molecular kinetic model proposed by Kumar and Kunzru [16] for naphtha pyrolysis is adopted. The model contains 18 species, 1 primary reaction and 21 secondary reactions.

The species equations are

$$\frac{\partial N_m}{\partial t}+\frac{V}{S}\frac{\partial N_m}{\partial l}-\frac{x_m}{M_m}\frac{\partial G}{\partial t}=\sum_{i\in \mathrm{REA}}\xi_{i,m}r_i,\quad m=1,2,\ldots,18 \tag{4}$$

where

$$r_i=r_i^+-r_i^-=K_{0,i}^+\mathrm{e}^{-E_i^+/\mathrm{RT}}\prod_{j\in \mathrm{REA}_i}N_j-K_{0,i}^-\mathrm{e}^{-E_i^-/\mathrm{RT}}\prod_{k\in \mathrm{RES}_i}N_k$$

$$x_m=\frac{N_m M_m}{\sum_{n\in \mathrm{COM}}N_n M_n+N_{\mathrm{H_2O}}M_{\mathrm{H_2O}}},\quad V=\frac{\mathrm{RT}(\sum_{m\in \mathrm{COM}}N_m+N_{\mathrm{H_2O}})}{P}$$

3.3. Energy model equations

Energy equation of the cracking gas is

$$\frac{\partial T}{\partial t}+\frac{V}{S}\frac{\partial T}{\partial l}=\frac{V}{S}\frac{K\pi D_{\mathrm{o}}(T_W-T)}{C_p}-\frac{\sum_{m\in \mathrm{COM}}\left(\Delta H_m\sum_{i\in \mathrm{REA}}\xi_{i,m}r_i\right)}{C_p} \tag{5}$$

where

$$C_p=\sum_m C_m N_m+C_{\mathrm{H_2o}}N_{\mathrm{H_2o}},\quad K=1\Big/\left(\frac{D_{\mathrm{o}}}{\chi(D_{\mathrm{o}}-2\delta_{\mathrm{W}}-2\delta_{\mathrm{C}})}+\frac{D_{\mathrm{o}}\delta_{\mathrm{W}}}{\lambda_{\mathrm{W}}(D_{\mathrm{o}}-\delta_{\mathrm{W}})}+\frac{D_{\mathrm{o}}}{\lambda_c(D_{\mathrm{o}}-2\delta_{\mathrm{W}}-\delta_{\mathrm{C}})}\right)$$

$\lambda_{\mathrm{W}}=a+bT_{\mathrm{W}}$, a and b are constant.

Energy equation of the tube wall is

$$\frac{\partial T_{\mathrm{W}}}{\partial t}=\frac{\sigma\alpha A_{cp}F[T_{\mathrm{g}}^4-T_{\mathrm{W}}^4]+1.8\cdot\sqrt[4]{T_{\mathrm{g}}-T_{\mathrm{W}}}A_s(T_{\mathrm{g}}-T_{\mathrm{W}})-K(T_{\mathrm{W}}-T)\pi D_{\mathrm{o}}}{G_{\mathrm{W}}C_{\mathrm{W}}} \tag{6}$$

where T_{g} conforms to quadratic function with reactor tube height [14].

4. DIFFERENCE SCHEME

4.1. Flow model equations

The difference scheme being fully Crank Nicolson for Equation (1) and fully implicit for Equation (3) has shown success for moderate time steps [19] and, hence, is used here. Thus, partial derivatives in Equations (1) and (3) are replaced by

$$\begin{aligned}&\frac{\partial P}{\partial t}=\frac{P_l^t-P_l^{t-1}}{\Delta t},\quad \frac{\partial G}{\partial l}=\frac{1}{2\Delta l}\left(\frac{G_{l+1}^t+G_{l+1}^{t-1}}{2}-\frac{G_{l-1}^t+G_{l-1}^{t-1}}{2}\right),\quad \text{Crank Nicolson}\\&\frac{\partial G}{\partial t}=\frac{G_l^t-G_l^{t-1}}{\Delta t},\quad \frac{\partial P}{\partial l}=\frac{P_{l+1}^t-P_{l-1}^t}{2\Delta l},\quad \text{fully implicit}\end{aligned} \tag{7}$$

DOI: 10.1002/fld

Equations (1) and (3) after cross differencing [19] and rearranging reduce to

$$-G_{l-1}^{t}+\frac{2\overline{M}_{l}^{t}S_{l}\Delta l}{\mathrm{RT}_{l}^{t}\Delta t}P_{l}^{t}+G_{l+1}^{t}=G_{l-1}^{t-1}+\frac{2\overline{M}_{l}^{t}S_{l}\Delta l}{\mathrm{RT}_{l}^{t}\Delta t}P_{l}^{t-1}-G_{l+1}^{t-1}$$

$$-P_{l}^{t}+\left(\frac{2\Delta l}{S_{l+1}\Delta t}+\frac{2\Delta l\mathrm{RT}_{l+1}^{t}f_{l+1}^{t}e_{l+1}|G_{l+1}^{t}|}{\overline{M}_{l+1}^{t}D_{l+1}S_{l+1}^{2}(P_{l}^{t}+P_{l+2}^{t})}\right)G_{l+1}^{t}+P_{l+2}^{t}$$

$$=\frac{2\Delta l}{S_{l+1}\Delta t}G_{l+1}^{t-1} \tag{8}$$

4.2. Reaction model equations

The Crank Nicolson scheme has a better accuracy for smaller time steps and hence is used here. Partial derivatives in Equation (4) is replaced by

$$\frac{\partial N_{m}}{\partial t}=\frac{N_{m,l}^{t}-N_{m,l}^{t-1}}{\Delta t}$$
$$\frac{\partial N_{m}}{\partial l}=\frac{N_{m,l}^{t}-N_{m,l-1}^{t}}{\Delta l} \tag{9}$$

Equation (4) after differencing and rearranging reduces to

$$N_{m,l}^{t}=\frac{S_{l-1}\Delta l\Delta t\overline{r}+\Delta t\overline{V}N_{m,l-1}^{t}+S_{l-1}\Delta lN_{m,l}^{t-1}}{S_{l-1}\Delta l+\overline{V}\Delta t}$$

$$+\frac{S_{l-1}\Delta l\overline{x}_{m}}{M_{m}(S_{l-1}\Delta l+\overline{V}\Delta t)}(G_{l}^{t}-G_{l}^{t-1}) \tag{10}$$

where

$$\overline{r}=\sum_{i}\xi_{i,m}\left[\frac{1}{2}\left(\frac{r_{i,l-1}^{t-1}+r_{i,l}^{t-1}}{2}+\frac{r_{i,l-1}^{t}+r_{i,l}^{t}}{2}\right)\right],\quad \overline{V}=\frac{1}{2}\left(\frac{V_{l-1}^{t-1}+V_{l}^{t-1}}{2}+\frac{V_{l-1}^{t}+V_{l}^{t}}{2}\right)$$

$$\overline{x}_{m}=\frac{1}{2}\left(\frac{x_{m,l-1}^{t-1}+x_{m,l}^{t-1}}{2}+\frac{x_{m,l-1}^{t}+x_{m,l}^{t}}{2}\right)$$

4.3. Energy model equations

The Crank Nicolson scheme for Equations (5) and (6) is used. Partial derivatives in Equations (5) and (6) are replaced by

$$\frac{\partial T}{\partial t}=\frac{T_{l}^{t}-T_{l}^{t-1}}{\Delta t},\quad \frac{\partial T}{\partial l}=\frac{T_{l}^{t}-T_{l-1}^{t}}{\Delta l},\quad \frac{\partial T_{\mathrm{W}}}{\partial t}=\frac{T_{\mathrm{W},l}^{t}-T_{\mathrm{W},l}^{t-1}}{\Delta t} \tag{11}$$

DOI: 10.1002/fld

Let

$$g=\frac{V}{S}\frac{K\pi D_{\mathrm{o}}(T_{\mathrm{W}}-T)}{C_p}-\frac{\sum_{m\in\mathrm{COM}}(\Delta H_m\sum_{i\in\mathrm{REA}}\xi_{i,m}r_i)}{C_p}$$

$$h=\frac{\sigma\alpha A_{cp}F[T_{\mathrm{g}}^4-T_{\mathrm{W}}^4]+1.8\cdot\sqrt[4]{T_{\mathrm{g}}-T_{\mathrm{W}}}A_s(T_{\mathrm{g}}-T_{\mathrm{W}})-K(T_{\mathrm{W}}-T)\pi D_{\mathrm{o}}}{G_{\mathrm{W}}C_{\mathrm{W}}}$$

then Equations (5) and (6) after differencing and rearranging reduce to

$$\begin{aligned}T_l^t&=\frac{S_{l-1}\Delta l T_l^{t-1}+\overline{V}\Delta t T_{l-1}^t+S_{l-1}\Delta t\Delta l\overline{g}}{S_{l-1}\Delta l+\overline{V}\Delta t}\\ T_{\mathrm{W},l}^t&=T_{\mathrm{W},l}^{t-1}+\overline{h}\Delta t\end{aligned}\tag{12}$$

where

$$\overline{g}=\frac{1}{2}\left(\frac{g_{l-1}^{t-1}+g_l^{t-1}}{2}+\frac{g_{l-1}^t+g_l^t}{2}\right),\quad \overline{h}=\frac{1}{2}\left(\frac{h_{l-1}^{t-1}+h_l^{t-1}}{2}+\frac{h_{l-1}^t+h_l^t}{2}\right)$$

5. SOLUTION ALGORITHM

The mathematical model after differencing is large-scale and highly coupled, which is difficult to solve it with traditional methods. The 'flow-reaction' decomposition strategy [21] is adopted to solve the model. The whole model is divided into flow block and reaction block to be solved, respectively, by an overall convergence program (note that the energy model equations are attributed to reaction block). Starting from the initialized fields, the flow block is solved first and then the reaction block equations are solved based on the previously calculated values of the flow variables. The calculation of flow and reaction blocks are then repeated until overall convergence is reached for the variables of both blocks. The convergence variables between flow and reaction blocks are the temperature (T), average molecular weight ($\overline{M}$) and average viscosity ($\overline{v}$) of the cracking gas. Let $\mathbf{X}^t=[T_1^t,\overline{M}_1^t,\overline{v}_1^t,T_2^t,\overline{M}_2^t,\overline{v}_2^t,\ldots,T_L^t,\overline{M}_L^t,\overline{v}_L^t]$, the schematic diagram of the decomposition algorithm is shown as Figure 1(a). The flow block is solved by the iteration algorithm proposed by Malik *et al.* [19] (see Appendix B), while the reaction block is solved by the direct iteration algorithm segment by segment along the tube length. Let $\mathbf{Y}_l^t=[T_l^t,T_{\mathrm{W},l}^t,N_{1,l}^t,N_{2,l}^t,\ldots,N_{18,l}^t]$, the schematic diagram of the algorithm for reaction block is shown as Figure 1(b).

6. SIMULATION RESULTS AND DISCUSSIONS

The proposed mathematical model and the decomposition algorithm are used to perform fluid dynamic simulation in the tubular reactor of a millisecond cracking furnace. The structure of the tubular reactor is shown in Figure 2, which is composed of two straight tubes, two elbows, one tee and one converge tube. The total length of the tubular reactor is 11.3 m, and the inner (outer) diameter of the straight tubes and converge tube are 0.0363 (0.0483) m and 0.0451 (0.0603) m, respectively. The cracking furnace totally contains 36 groups of the above tubular reactor. Naphtha is the main material for the millisecond cracking furnace.

DOI: 10.1002/fld

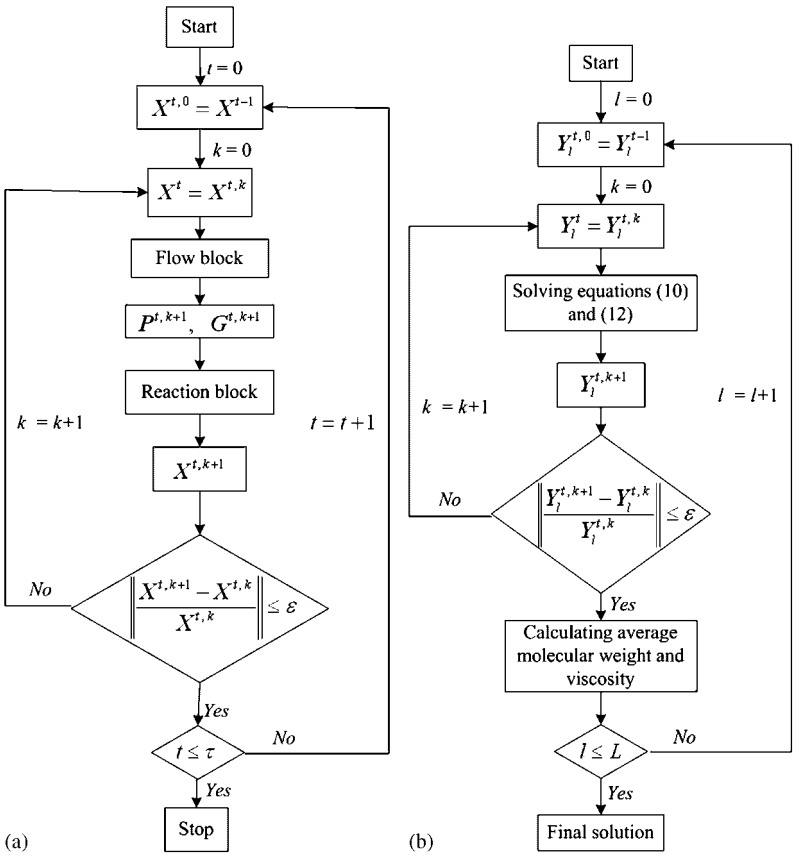

Figure 1. Schematic diagrams of the decomposition algorithm (a) and the algorithm for reaction block (b).

6.1. Benchmark of static simulation

Let

$$\frac{\partial P}{\partial t}=0,\quad \frac{\partial G}{\partial t}=0,\quad \frac{\partial N_m}{\partial t}=0,\quad \frac{\partial T}{\partial t}=0\quad \text{and}\quad \frac{\partial T_W}{\partial t}=0$$

of the dynamic model proposed in this paper, we can obtain the mathematical model for static simulation presented by Xu *et al.* [14]. In the static simulation, the inlet pressure and flue gas temperature are the adjustment variables for reaching the given outlet pressure and temperature [14]. In the Kumar molecular kinetic model, the selectivities of the first-order reaction are sensitive on the properties of the cracking naphtha. Hence, the selectivities need to adjust when the cracking material changes. In the cases studies, the same naphtha is used, the properties of which are listed in Table I. Using the naphtha, three cases at different cracking conditions are listed in Table II. Case 1 and case 2 are industrial cases, while the base case is constructed for the next dynamic simulation by averaging the cracking conditions of cases 1 and 2. For the given naphtha, after adjusting the selectivities of the first-order reaction, the results of static simulation for the tubular

DOI: 10.1002/fld

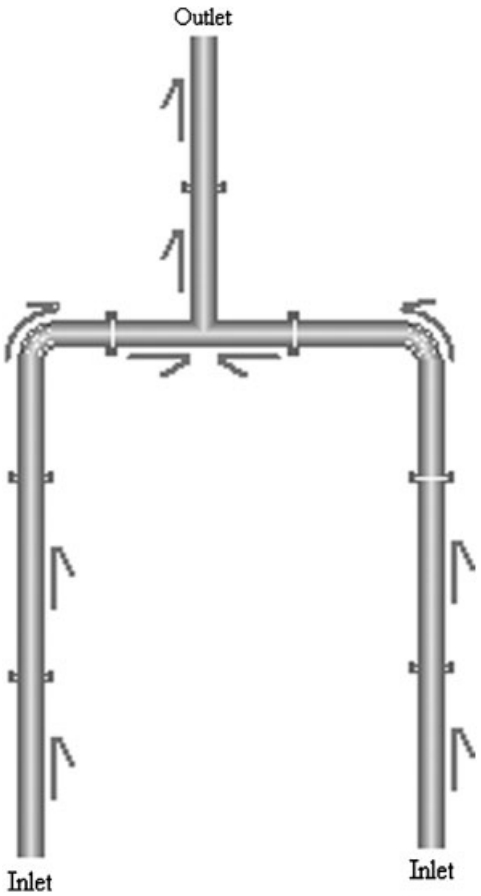

Figure 2. Structure of the tubular reactor in the millisecond cracking furnace.

Table I. Properties of the used naphtha.

POINA weight fraction		ASTM distillation range (°C)	
P%	38.49	IBP	35.9
I%	30.28	10%	62.7
N%	24.82	30%	85.6
O%	0.02	50%	101.3
A%	6.37	70%	118.0
Density (g/cm^3, 20°C)	0.7048	90%	137.8
		FBP	154.0

reactor in three cases are listed in Table III. The errors of ethylene, propylene and methane obtained by the static simulation are less than 1.0%, which indicate that the static mathematical model is reliable.

DOI: 10.1002/fld

Table II. Cracking conditions in the tubular reactor.

Cracking conditions	Case 1	Case 2	Base case
Total inlet feedrate (kg/h)	311.2	266.4	288.8
Water oil ratio	0.55	0.6	0.58
Inlet temperature (°C)	625.0	632.0	628.0
Outlet temperature (°C)	855.0	861.0	858.0
Outlet pressure (Pa)	160000	142000	150000
Coke thickness (m)	0	0	0

Table III. Results of static simulation.

	Case 1		Case 2		Base case
Products	Simulation result (wt%)	Experimental result (wt%)	Simulation result (wt%)	Experimental result (wt%)	Simulation result (wt%)
H_2	1.22	1.23	1.23	1.22	1.20
CH_4	19.90	20.09	19.87	19.60	19.52
C_2H_6	2.82	2.85	2.54	2.49	2.58
C_2H_4	31.32	31.49	31.69	31.84	31.15
C_3H_8	0.42	0.46	0.41	0.38	0.42
C_3H_6	10.92	11.05	10.89	10.73	11.02
C_4H_8	2.69	2.79	2.70	2.63	2.80
C_4H_6	5.33	5.06	5.51	5.80	5.39
C_4H_{10}	0.31	0.35	0.30	0.28	0.35

The adjusted flue gas temperature curves are depicted in Figure 3, which accord with the industrial measured data on the whole. Subsequently, the same naphtha, cracking conditions and flue gas temperature distribution of the base case are used in the dynamic simulation and the results of the static simulation are given as initial values of the dynamic simulation.

6.2. Results of dynamic simulation

The dynamic simulation is implemented by a conventional procedure on a personal computer (CPU Intel 2.66G, RAM 2G). The tubular reactor is equally subdivided into 625 slight segments. To investigate the dynamic process in the tubular reactor, the ±5% step disturbance of inlet feedrate is given based on the results of static simulation for the base case. The disturbed inlet feedrate lay in the interval 266.4–311.2 kg/h that will not debase the applicability of the mathematical model.

6.2.1. Dynamic curve of outlet parameters in a short time. The parameters of dynamic simulation are set as follows: time step $\Delta t = 0.001$ s, total number of time steps $\tau = 1000$ and tolerance $\varepsilon = 10^{-4}$. It needs about 5–6 min to implement the dynamic simulation procedure once. Given a step disturbance of inlet feedrate, the dynamic curve of outlet weight flowrate, coil outlet temperature (COT), weight content of ethylene and propylene are depicted in Figure 4.

From the figure, under the step disturbance of inlet feedrate, the outlet parameters fluctuate obviously in a short time (<0.5 s). These indicate that the dynamic process is transitory in the tubular reactor, which is in accordance with industrial experiences because the tubular reactor

DOI: 10.1002/fld

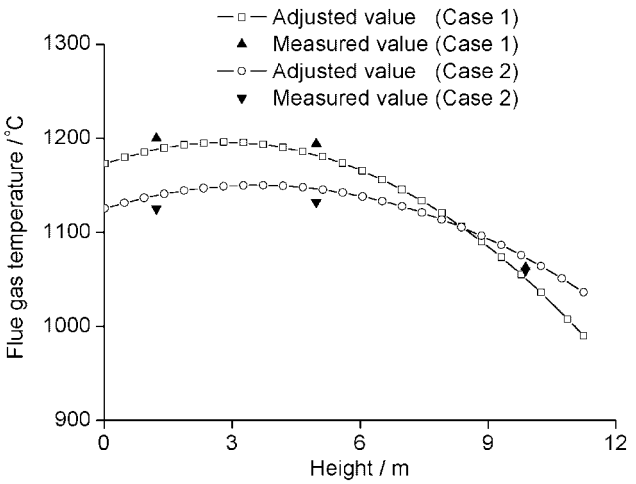

Figure 3. Flue gas temperature curves in two industrial cases.

has a short residence time. As shown in Figures 4(b)–(d), the outlet ethylene weight content and COT decrease with inlet feedrate augments, while the outlet propylene weight content increases with inlet feedrate augments. These results are also in accordance with industrial experiences. Figures 4(a) and (b) show the COT first rises then descends as the flowrate increases at the beginning of the dynamic process, which can be interpreted. The increscent flow rate presents a higher heat capacity that leads to a drop of the COT, meanwhile it shows a better performance of heat transfer and the less reactive endotherm that results in a rise of the COT. Hence, the final change trend of COT is up to the trade-off of multi-type factors. Under positive and negative step disturbances, the dynamic processes of outlet weight flowrate, COT, outlet weight content of ethylene and propylene are symmetrical basically, as shown in Figure 4.

The dynamic process of fluid flow in the different place of the tubular reactor is shown in Figure 5, which indicates that fluid flow changes increasingly from inlet to outlet of the tubular reactor.

6.2.2. Dynamic curve of outlet parameters in a longer time. Because the heat capacity of the tube wall is hundreds of times greater than that of the cracking gas, it needs a longer time to reach the new steady value of the tube wall temperature. Thus, outlet parameters except weight rate tardily change until reach to the new steady value after the fast fluctuating in a short time. Figure 6 shows the dynamic curve of COT and ethylene weight content in a longer time.

In addition, the distribution of temperature and average molecular weight of the cracking gas along the tube length are depicted in Figure 7, respectively. These indicate that the fluid flow is nonisothermal and variational molecule in the tubular reactor due to heat transfer and reaction.

Here, only a case of a millisecond cracking furnace is presented. However, the proposed mathematical model is developed not only for the coil of a millisecond cracking furnace. It is also applicable for other cracking coils such as the USC cracking coil of S.W. Company.

DOI: 10.1002/fld

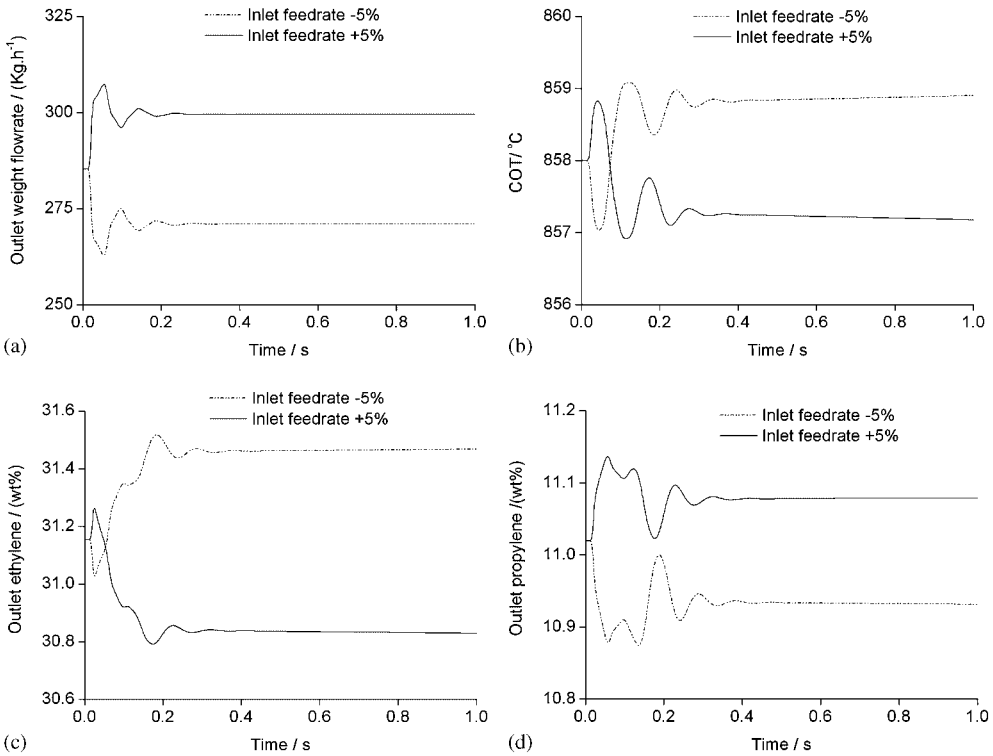

Figure 4. Dynamic curves of outlet weight flowrate (a), COT (b), outlet ethylene weight content (c) and outlet propylene weight content (d).

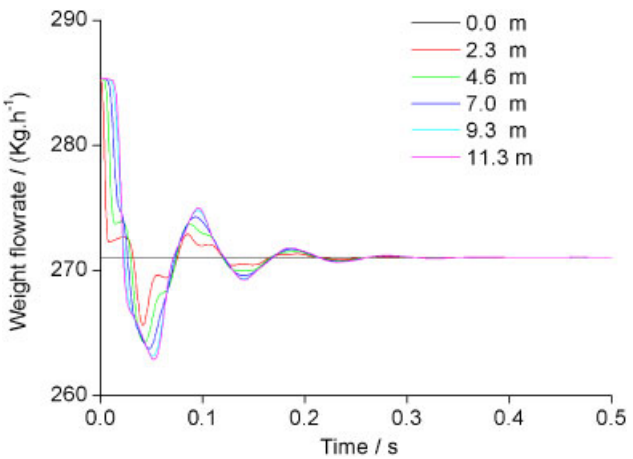

Figure 5. Dynamic process of weight flowrate in the tubular reactor (inlet feedrate: −5%).

DOI: 10.1002/fld

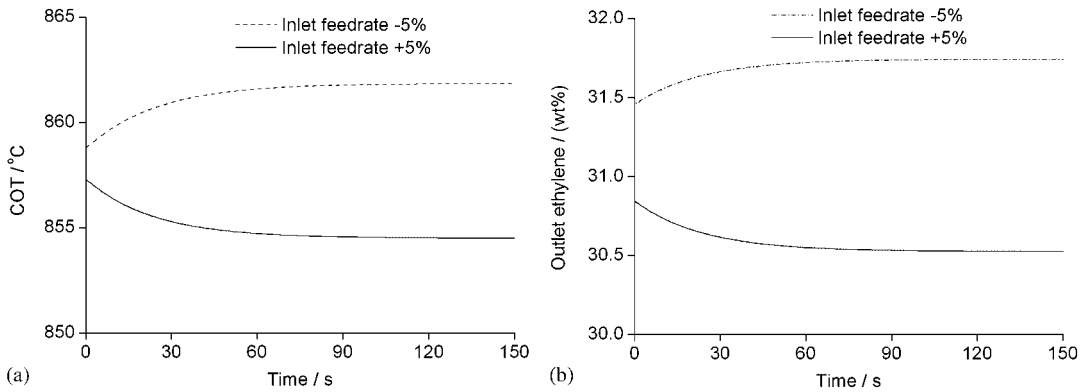

Figure 6. Dynamic curves of COT (a) and outlet ethylene weight content (b).

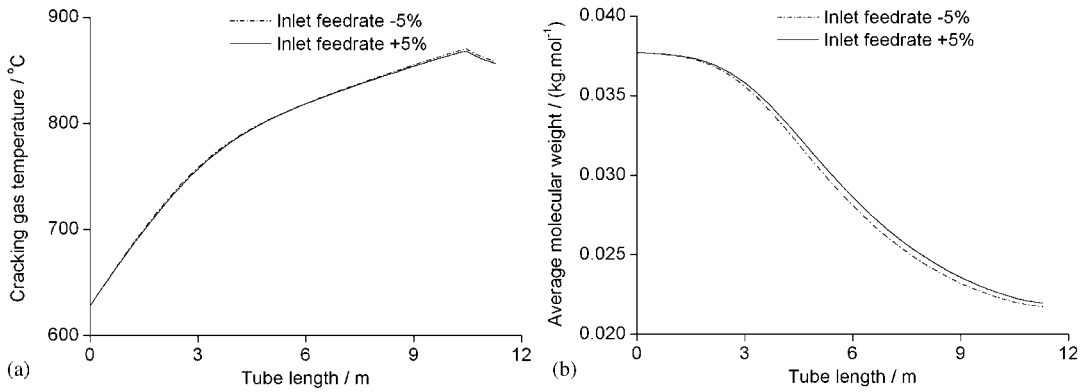

Figure 7. Distributions of cracking gas temperature (a) and average molecular weight (b) in the tubular reactor at new steady states.

7. ALGORITHM DISCUSSIONS

Difference scheme, time step and the overall iteration efficiency are discussed here.

7.1. Difference scheme in reaction block

Explicit, Crank Nicolson and implicit schemes for the reaction and energy model equations are compared in Figure 8. The results indicate that Crank Nicolson scheme has a better accuracy.

7.2. Time step selection

Time step selection has an important impact in the accuracy and efficiency of the dynamic simulation. A smaller time step can improve the accuracy but will decrease the efficiency, contrarily a larger time step will improve the efficiency but lose the accuracy. Figure 9 depicts the COT results of dynamic simulation in the tubular reactor with three time steps and the CPU time consumed

DOI: 10.1002/fld

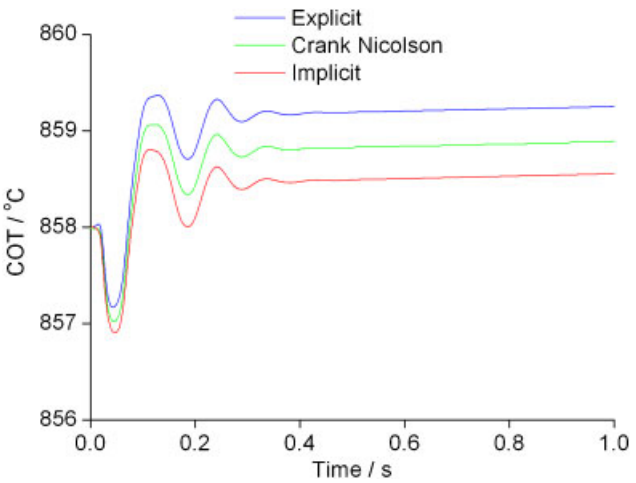

Figure 8. Comparisons for three difference schemes.

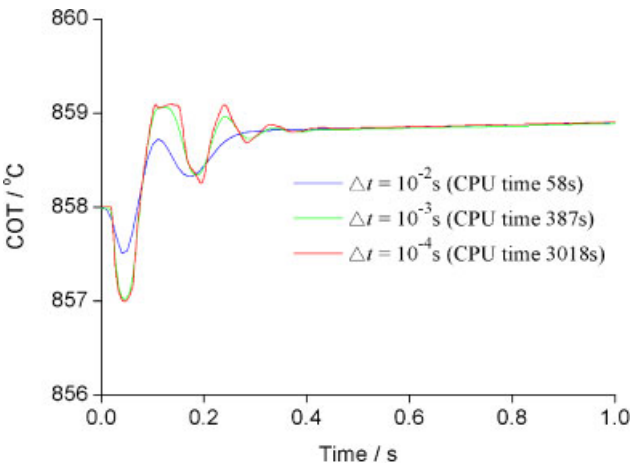

Figure 9. Results of the dynamic simulation with different time steps.

with each time step is also listed in the figure. The results show that the appreciate time step (10^{-3} s) has a better performance in both accuracy and efficiency in this dynamic simulation.

7.3. Overall iteration efficiency

The efficiency of overall iteration in the decomposition algorithm is concerned. Figure 10 lists the overall error changes as iteration number at different time in the dynamic simulation, which indicates a good efficiency of the overall iteration. Commonly, it only needs several times to reach the given tolerance.

DOI: 10.1002/fld

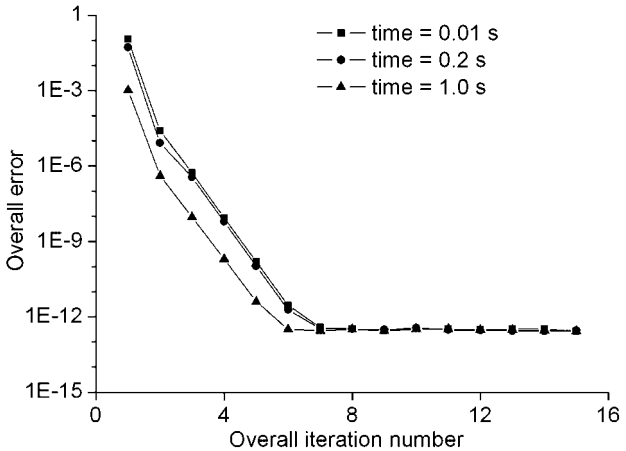

Figure 10. Efficiency of overall iteration in the decomposition algorithm.

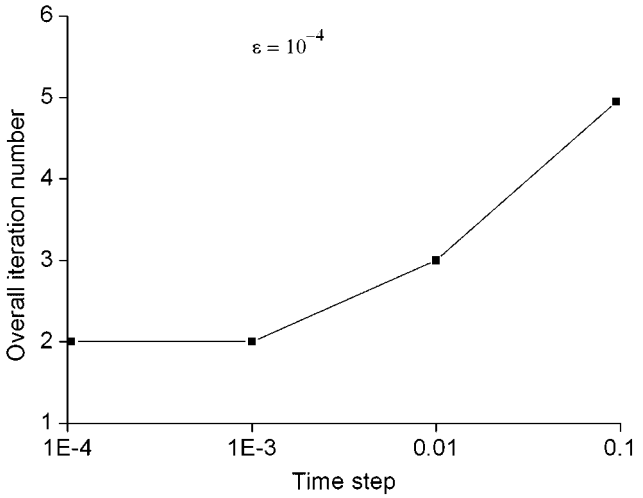

Figure 11. Comparisons of overall iteration number with different time steps.

Finally, the efficiency of the overall iteration under different time steps is investigated. Figure 11 presents the overall iteration number changes as time step. The results indicate that different time steps do not have a great impact in the efficiency of the overall iteration.

8. CONCLUSIONS

This paper presents a comprehensive mathematical model containing equations for mass, momentum and heat transfer combined with Kumar molecular kinetic model to describe dynamic

DOI: 10.1002/fld

behaviors of fluid flow, heat transfer and reaction in the tubular reactor of industrial cracking furnace. The 'flow-reaction' decomposition strategy is adopted to solve the model for performing the fluid dynamic simulation coupled with heat transfer and reaction in the tubular reactor by a conventional procedure. The mathematical model and the decomposition algorithm are successfully applied to the fluid dynamic simulation for the tubular reactor of a millisecond industrial cracking furnace. The results of dynamic simulation reveal the various transient behaviors of fluid flow, temperature change and species content variation in the tubular reactor under the step disturbance of inlet feedrate. The unsteady-state fluid flow process in the tubular reactor is quite transitory under the disturbance, which is less than 0.5 s. The algorithm investigations indicate that the decomposition algorithm has a good performance in the fluid dynamic simulation for the tubular reactor of industrial cracking furnaces. Based on this work, the next further investigation will be the comprehensive dynamic simulation of the whole industrial cracking furnace.

APPENDIX A: KUMAR MOLECULAR KINETIC MODEL

No.	Reaction equation	E (MJ/kmol)	K_0 (s^{-1} or m^3/kmol s)
1	$CxHy \rightarrow z_1H_2 + z_2CH_4 + z_3C_2H_6 + z_4C_2H_4 + z_5C_3H_8 + z_6C_3H_6 + z_7C_4H_8 + z_8C_4H_6 + z_9C_4H_{10} + z_{10}C_4'$	219.78	6.565×10^{11}
2	$C_2H_6 \leftrightarrow C_2H_4 + H_2$	272.58	4.652×10^{13}
3	$C_3H_6 \leftrightarrow C_2H_2 + CH_4$	273.08	7.284×10^{12}
4	$C_2H_2 + C_2H_4 \rightarrow C_4H_6$	172.47	1.026×10^{12}*
5	$2C_2H_6 \rightarrow C_3H_8 + CH_4$	272.75	3.75×10^{12}
6	$C_2H_4 + C_2H_6 \rightarrow C_3H_6 + CH_4$	252.60	7.083×10^{13}*
7	$C_3H_8 \leftrightarrow C_3H_6 + H_2$	214.39	5.888×10^{10}
8	$C_3H_8 \rightarrow C_2H_4 + CH_4$	211.51	4.692×10^{10}
9	$C_3H_8 + C_2H_4 \rightarrow C_2H_6 + C_3H_6$	246.87	2.536×10^{13}*
10	$2C_3H_6 \rightarrow 3C_2H_4$	268.23	7.386×10^{12}
11	$2C_3H_6 \rightarrow 0.3C_nH_{2n-6} + 0.14C_6 + +3CH_4$	237.84	2.424×10^{11}
12	$C_3H_6 + C_2H_6 \rightarrow 1-C_4H_8 + CH_4$	250.84	1.0×10^{14}*
13	n-$C_4H_{10} \rightarrow C_3H_6 + CH_4$	249.30	7.0×10^{12}
14	n-$C_4H_{10} \rightarrow 2C_2H_4 + H_2$	295.44	7.0×10^{14}
15	n-$C_4H_{10} \rightarrow C_2H_4 + C_2H_6$	256.28	4.099×10^{12}
16	n-$C_4H_{10} \leftrightarrow 1-C_4H_8 + H_2$	260.66	1.637×10^{12}
17	$1-C_4H_8 \rightarrow 0.41C_nH_{2n-6} + 0.19C_6^+$	212.05	2.075×10^{11}
18	$1-C_4H_8 \leftrightarrow H_2 + C_4H_6$	209.0	1.0×10^{10}
19	$C_2H_4 + C_4H_6 \rightarrow B + 2H_2$	144.46	8.385×10^{9}*
20	$C_4H_6 + C_3H_6 \rightarrow T + 2H_2$	148.98	9.74×10^{8}*
21	$C_4H_6 + 1-C_4H_8 \rightarrow EB + 2H_2$	242.31	6.4×10^{14}*
22	$C_4H_6 + C_4H_6 \rightarrow ST + 2H_2$	124.40	1.51×10^{9}*

Notation: B—benzene, T—toluene, EB—ethylbenzene, ST—cinnamene.
'*'—second order reaction.
'$\rightarrow$'—irreversible reaction, '$\leftrightarrow$'—reversible reaction.

DOI: 10.1002/fld

APPENDIX B: ALGORITHM FOR FLOW BLOCK

Equations (8) are rewritten as follows:

$$-G_{l-1}^{t}+\frac{2M_l^{t*}S_l\Delta l}{\mathrm{RT}_l^{t*}\Delta t}P_l^{t}+G_{l+1}^{t}=G_{l-1}^{t-1}+\frac{2M_l^{t*}S_l\Delta l}{\mathrm{RT}_l^{t*}\Delta t}P_l^{t-1}-G_{l+1}^{t-1}$$
$$-P_l^{t}+\left(\frac{2\Delta l}{S_{l+1}\Delta t}+\frac{2\Delta l\mathrm{RT}_{l+1}^{t*}f_{l+1}^{t*}e_{l+1}|G_{l+1}^{t*}|}{M_l^{t*}D_{l+1}S_{l+1}^{2}(P_l^{t*}+P_{l+2}^{t*})}\right)G_{l+1}^{t}+P_{l+2}^{t}$$
$$=\frac{2\Delta l}{S_{l+1}\Delta t}G_{l+1}^{t-1} \tag{B1}$$

where superscript '$*$' refers to the values of variables at current time step, but at previous iteration. Let $\mathbf{X}_l^t=[P_1^t, G_2^t, P_3^t, G_4^t, \ldots, P_{L-2}^t, G_{L-1}^t]$, be the set of Equations (B1) written in matrix form for the tubular reactor is

$$\mathbf{AX}=\mathbf{B} \tag{B2}$$

which is of the form

$$\begin{bmatrix}
a_1 & 1 & & & & & & & & \\
-1 & a_2 & 1 & & & & & & & \\
 & -1 & a_3 & 1 & & & & & & \\
 & & \cdot & \cdot & \cdot & & & & & \\
 & & & \cdot & \cdot & \cdot & & & & \\
 & & & & -1 & a_i & 1 & & & \\
 & & & & & \cdot & \cdot & \cdot & & \\
 & & & & & & \cdot & \cdot & \cdot & \\
 & & & & & & & -1 & a_{L-2} & 1 \\
 & & & & & & & & -1 & a_{L-1}
\end{bmatrix}
\begin{bmatrix} P_1^t \\ G_2^t \\ P_3^t \\ \cdot \\ \cdot \\ G_i^t \\ \cdot \\ \cdot \\ P_{L-2}^t \\ G_{L-1}^t \end{bmatrix}
=
\begin{bmatrix} b_1+G_0 \\ b_2 \\ b_3 \\ \cdot \\ \cdot \\ b_i \\ \cdot \\ \cdot \\ b_{L-2} \\ b_{L-1}-P_L \end{bmatrix}$$

where

$$a_i=\frac{2M_l^{t*}S_l\Delta l}{\mathrm{RT}_l^{t*}\Delta t},\quad b_i=G_{l-1}^{t-1}+\frac{2M_l^{t*}S_l\Delta l}{\mathrm{RT}_l^{t*}\Delta t}P_l^{t-1}-G_{l+1}^{t-1},\quad i \text{ is odd}$$

$$a_i=\left(\frac{2\Delta l}{S_{l+1}\Delta t}+\frac{2\Delta l\mathrm{RT}_{l+1}^{t*}f_{l+1}^{t*}e_{l+1}|G_{l+1}^{t*}|}{M_l^{t*}D_{l+1}S_{l+1}^{2}(P_l^{t*}+P_{l+2}^{t*})}\right),\quad b_i=\frac{2\Delta l}{S_{l+1}\Delta t}G_{l+1}^{t-1},\quad i \text{ is even}$$

A is a tridiagonal matrix, thus Equation (B2) is easily solved by Gauss elimination method. The algorithm for flow block is shown as Figure B1.

DOI: 10.1002/fld

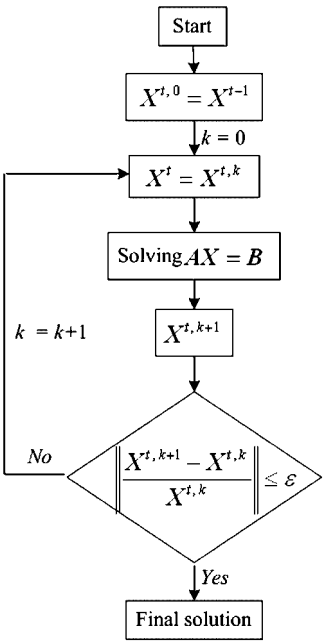

Figure B1. Schematic graph of the iterative algorithm in flow block.

NOMENCLATURE

Sets

COM	set of species in Kumar molecular kinetic model
REA	set of reactions in Kumar molecular kinetic model
REA_i	set of reactants in the ith reaction
RES_i	set of resultants in the ith reaction

Subscripts/superscripts

H_2O	water
i	reaction
j	reactant
k	resultant
l	segment
m	species
n	species
t	time
$+$	positive reaction
$-$	reverse reaction

Symbols used

A_{cp} (m^2)	equivalent flat area
A_s (m^2)	convective heat transfer area

DOI: 10.1002/fld

C (J/mol K)	species heat capacity
C_p (J/mol K s)	cracking gas average heat capacity flowrate
C_{W} (J/kg K)	tube wall heat capacity
D (m)	actual reactor inner diameter
D_o (m)	reactor outer diameter
E (J/mol)	activation energy
e (dimensionless)	equivalent reduced factor
f (dimensionless)	Fanning friction factor
F (dimensionless)	total exchange factor
G (kg/s)	total cracking gas mass flowrate
G_{W} (kg)	tube wall weight
ΔH (J/mol)	standard molar formation enthalpy
K (W/m k)	total heat transfer coefficient
K_0 (s^{-1}, m^3/mol s)	reaction rate constant
L (dimensionless)	total segments
Δl (m)	segment length
M (kg/mol)	molecular weight
$\overline{M}$ (kg/mol)	average molecular weight
N (mol/s)	species molar flowrate
P (Pa)	cracking gas pressure
R (J/mol K)	gas constant, 8.314
r (mol/s^2)	reaction rate
Re (dimensionless)	Reynolds number
S (m^2)	actual reactor currency area
T (K)	cracking gas temperature
T_{W} (K)	tube wall temperature
T_{g} (K)	flue gas temperature
Δt (s)	time step
V (m^3/s)	cracking gas average volume flowrate
x (dimensionless)	species weight content

Greek symbols

α (dimensionless)	view factor
χ (W/m K)	cracking gas heat transfer coefficient
δ_C (m)	coke thickness
δ_W (m)	tube wall thickness
ε (dimensionless)	error tolerance
λ_C (W/m K)	coke conductivity factor
λ_W (W/m^2 K)	tube wall conductivity factor
σ (W/m^2 K^4)	Stefan–Boltzmann constant, 5.7×10^{-8}
τ (dimensionless)	total number of time steps
υ (Pa s)	viscosity
$\overline{\upsilon}$ (Pa s)	average viscosity
ξ (dimensionless)	stoichiometric coefficient

DOI: 10.1002/fld

ACKNOWLEDGEMENTS

This work is supported by the National Scientific and Technical Supporting Programs in the 11th Five-year Plan (No. 611408001).

REFERENCES

1. Dente M, Ranzi E, Goossens GA. Detail prediction of olefin yields from hydrocarbon pyrolysis through a fundamental simulation model (SRYRO). *Computers and Chemical Engineering* 1979; **3**:61–72.
2. Towfighi J, Nazari H, Karimzadeh R. Development of mechanistic model for pyrolysis of naphtha. *APCCHE/CHEMECA93*, vol. 3. 1993; 337–342.
3. Joo E, Lee K, Lee M, Park S. CRACKER-a PC-based simulator for industrial cracking furnaces. *Computers and Chemical Engineering* 2000; **24**:1523–1528.
4. van Goethem MWM, Kleinendorst FI, van Leeuwen C, van Velzen N. Equation-based SPYRO model and solver for the simulation of the steam cracking process. *Computers and Chemical Engineering* 2001; **25**:905–911.
5. Niaei A, Towfighi J, Sadrameli SM, Karimadeh R. The combined simulation of heat transfer and pyrolysis reactions in industrial cracking furnaces. *Applied Thermal Engineering* 2004; **24**:2251–2265.
6. Heynderickx GJ, Oprins AJM, Marin GB, Dick E. Three-dimensional flow patterns in cracking furnaces with long-flame burners. *AICHE Journal* 2001; **47**(2):388–400.
7. Lan X, Gao J, Xu C, Zhang H. Numerical simulation of transfer and reaction processes in ethylene furnaces. *Chemical Engineering Research and Design* 2007; **85**(12):1565–1579.
8. Shahrokhi M, Nedjati A. Optimal temperature control of propane thermal cracking reactor. *Industrial Engineering Chemistry Research* 2002; **41**(25):6572–6578.
9. Masouemi ME, Sadrameli SM, Towfighi J, Niaei A. Simulation, optimization and control of a thermal cracking furnace. *Energy* 2006; **31**(4):516–527.
10. Ghashghaee M, Karimzadeh R. Dynamic modeling and simulation of steam cracking furnaces. *Chemical Engineering and Technology* 2007; **30**(7):835–843.
11. Shah JJ, Fox RO. Computational fluid dynamics simulation of chemical reactors: application of in situ adaptive tabulation to methane thermochloriination chemistry. *Industrial Engineering Chemistry Research* 1999; **38**: 4200–4212.
12. Gobin A, Neau H, Simonin O, Llinas JR, Reiling V, Selo JL. Fluid dynamic numerical simulation of a gas phase polymerization reactor. *International Journal for Numerical Methods in Fluids* 2003; **43**:1199–1220.
13. Khopkar AR, Kasat GR, Pandit AB, Ranade W. Computational fluid dynamics simulation of the solid suspension in a stirred slurry reactor. *Industrial Engineering Chemistry Research* 2006; **45**(12):4416–4428.
14. Xu Q, Chen B, He X. A fast simulation algorithm for industrial cracking furnaces. *Hydrocarbon Processing* 2002; **81**(12):65–68.
15. Joo E, Park S. Pyrolysis reaction mechanism for industrial naphtha cracking furnaces. *Industrial Engineering Chemistry Research* 2002; **40**:2409–2415.
16. Kumar P, Kunzru D. Modeling of naphtha pyrolysis. *Industrial Engineering Chemistry Process Design and Development* 1985; **24**:774–782.
17. Han YL, Xiao R, Zhang MY. Combustion and pyrolysis reactions in a naphtha cracking furnace. *Chemical Engineering and Technology* 2007; **30**(1):112–120.
18. Hu YF, Xu YM, He X. Modeling and simulation of naphtha pyrolysis process. *Petroleum Processing and Petrochemicals* 2004; **35**(5):57–62.
19. Malik MN, Afzal M, Tariq GF, Ahmed N. Mathematical modeling and computer simulation of transient flow in centrifuge cascade pipe network with optimizing techniques. *Computers and Mathematics with Applications* 1998; **36**(4):63–76.
20. Wang SH, He XO. *Ethylene Technique*. Sinopec Press: Beijing, 2000.
21. Asit KD, Edward B, Guy BM, Geraldine JH. Three-dimensional simulation of a fluid catalytic cracking riser reactor. *Industrial Engineering Chemistry Research* 2003; **42**:2602–2617.

DOI: 10.1002/fld